Design of a Novel Integrated Ultrasonic Tool Holder for Friction Stir Welding

Jianzhong Ju
Harbin Institute of Technology Shenzhen
Zhili Long (longzhili@hit.edu.cn)
Harbin Institute of Technology Shenzhen
Shuyuan Ye
Harbin Institute of Technology Shenzhen
Yongzhi Liu
Harbin Institute of Technology Shenzhen
Heng Zhao
Harbin Institute of Technology Shenzhen

Research Article

Keywords: friction stir welding, ultrasonic transducer, modal analysis, pre-tightening force

Posted Date: January 13th, 2022

DOI: https://doi.org/10.21203/rs.3.rs-1250127/v1

Design of a Novel Integrated Ultrasonic Tool Holder for Friction Stir Welding

Ju Jianzhong[1], Long Zhili[1*], Ye Shuyuan[1], Liu Yongzhi[1], Zhao Heng[1]

[1] Department of Mechanical Engineering and Automation, Harbin Institute of Technology (Shenzhen), Shenzhen 518055, China

[*]Corresponding author: Zhili Long. E-mail address: longzhili@hit.edu.cn (Long Zhili).

Abstract

Ultrasonic vibration used in friction stir welding (FSW) has shown advantages in reducing welding defects and improving welding quality. How to design an ultrasonic tool holder is a challenge because the holder is rotating in a confined space. In this study, we design a 20 kHz integrated ultrasonic tool holder in FSW. This novel configuration can be applied in general machining equipment. The elastic modulus is measured by non-destructive acoustic testing to attain the precise frequency. Three FSW transducers with alloy steel are designed by the modal analysis and the transducer prototypes are fabricated. The effect of pre-tightening force on transducer frequency is investigated, where the prestress of the piezoelectric stack instead of the torque is tested to achieve an optimal working frequency. The vibration of the transducers is measured by a Doppler Vibrometer System. It proved that the resonant frequencies are well consistent between simulation model and the experiment by the elastic modulus testing and the pre-tightening optimization. Moreover, the experiment demonstrates that the vibration amplitude is significantly different, even in a slight difference of steel material properties are adopted. The dynamic performance of the designed transducers is acceptable by the vibration measurement.

Keywords: friction stir welding; ultrasonic transducer; modal analysis; pre-tightening force

1 Introduction

Friction stir welding (FSW), a solid-state welding, has been widely used in a variety of fields such as aerospace, automobile, power electronics [1-3]. FSW has outstanding advantages in controlling welding defects, improving joint strength and fatigue properties [4, 5]. In FSW process, heat generation and material flow are necessary to achieve the high-quality welded joints, which also cause some issues such as high welding load and sharp tool wear. Nowadays, many optimized approaches such as thermal energy-assisted FSW [6-8] and ultrasonic vibration friction stir welding (UVFSW) [9, 10] have been proposed to improve the welding performance.

Ultrasonic vibration used in FSW is benefit to the plastic flow, mechanical properties of joints, and reduce welding defects [11-13]. Currently, researchers and engineers have developed various ultrasonic FSW devices. These devices can be divided into two configurations, where one is that the ultrasonic vibration is applied into the pin along the vertical and horizontal direction, and the other is that the ultrasonic energy is applied into the workpiece. Park [14] applied ultrasonic vibration to the pin through the lateral coupling bearing, which proved that ultrasonic energy could decrease the welding defects and enhance the mechanical properties of the joint. However, the ultrasonic energy was dissipated into other paths. Kumar [15, 16] improved Park's device to increase the energy transfer efficiency. He [17] developed a UVFSW system that integrated the transducer into the rotating fixture, which could efficiently apply ultrasonic energy to the weld nugget zone through the pin. Amini [18, 19] achieved the same rotary ultrasonic vibration mode and applied in shorter welding plates by refitting the lathe. In the second configuration, the ultrasonic vibration generated by lateral transducer makes the workpiece vibrate in high frequency. Wu [20] designed an inclined ultrasonic device in which the ultrasonic wave was propagated to the workpiece. Hu [21] accomplished an ultrasonic transmission device which can make ultrasound focus into the bottom of the workpiece. Strass [22] developed an ultrasonic rolling seam oscillator to apply vibration on the advancing side. Tarasov presented that an ultrasonic transducer was directly connected to the workpiece through a bolt structure [23]. In summary, the first configuration is that the ultrasonic component is complicated in structure, high mass and large volume, which cannot meet the confined space requirement. In the second configuration, there is a distance difference between the ultrasonic head and the pin, which can cause the ultrasonic energy dissipation because of the propagation attenuation.

The piezoelectric transducers are the critical component in ultrasonic machining. Small amplitude with resonant frequency is generated by the piezoelectric elements, and then is amplified to the tool tip by a horn. The resonant frequency and the vibration amplitude are the key parameters which influence the material processing and quality [24]. The resonant frequency is determined by the geometric construction and material properties, which is calculated by the mechanical equivalent circuit and finite element [15, 25, 26]. He [27] indicated that the ultrasonic properties of alloys were closely related to the elastic modulus. The increase of elastic modulus can decrease the vibration amplitude. To obtain the high energy conversion efficiency, many optimization approaches such as changing the position of the piezoelectric element [24, 28], the structure design for flange mounting [29] and fabrication technique, were proposed. The optimal pre-tightening force can significantly improve the frequency and vibration output of the transducer [30], which can avoid the cracks or degradation in piezoelectric stack. In general, the pre-tightening torque is controlled by a digital torque wrench. The optimal torque for transducer varies greatly with the

material composition and the size of piezoceramics. However, the optimal prestress of the piezeceramics is not related to its structure dimensions, which is benefit to make a precise control to resonant frequency.

In this study, a novel integrated ultrasonic tool holder with the advantage of compact structure, low mass and flexible replacement, is developed to meet with the FSW process. The transmission of ultrasonic energy is improved to the welding area. Firstly, the structure of ultrasonic transducer is designed based on the FSW characteristics. The elastic modulus of the material is measured by the non-destructive acoustic testing. The structural size of transducer is determined by finite element method using the measured material properties. FSW transducers of three steel alloy are fabricated and tested. The error of designed frequency by non-destructive acoustic wave is analyzed. On the other hand, the effect of prestress on the resonant frequency and the impedance is investigated to determine the appropriate prestress. Finally, the transducer vibration is tested to ensure the machining requirements. The amplitude outputs of transducers with different materials are compared.

2 Structure design

The configuration of ultrasonic FSW device is designed in Fig. 1. The ultrasonic generator can provide 15 kHz to 30 kHz AC excitation signals of different frequencies with 2000 Watt output power. The high frequency electrical signal is transmitted to the transducer through the slip ring. The piezoelectric ceramic stack is excited at the natural frequency of the transducer and amplifies the vibration by the horn. An external flange on the vibration node of the transducer is connected with the BT40 tool holder. Our self-developed ultrasonic generator has the functions such as frequency sweeping and searching automatically the resonant frequency and impedance, and real time tracking to the dynamics frequency for resonant vibration.

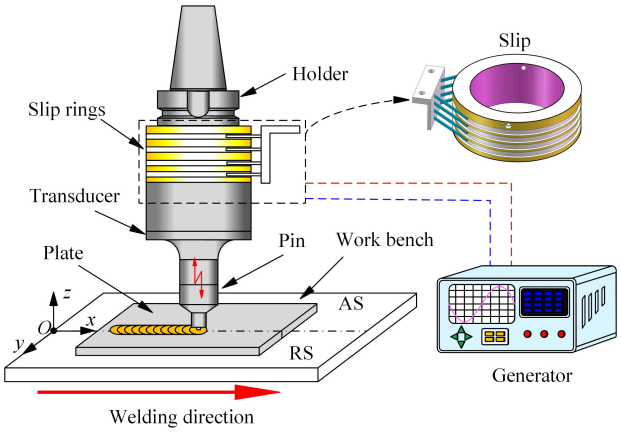

Fig. 1 Ultrasonic FSW configuration

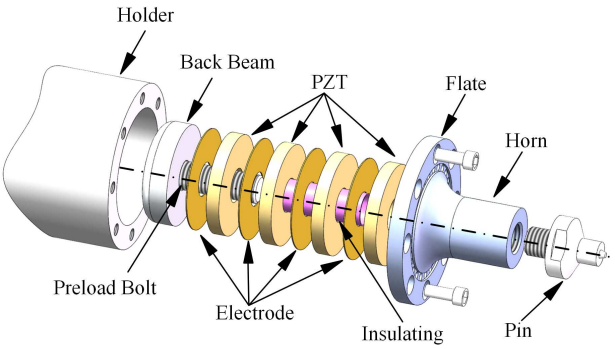

Fig. 2 Structure of the FSW transducer

The transducer in FSW includes the back plate, piezoceramics stacks, horn and pin. The piezoceramics stacks consist of four identical piezoceramics and two sets of copper electrode. These components are clamped by a pre-tightening screw. To realize the flexible replacement of the pin, the front end of the horn and the pin are connected by threads. Through modal simulation, the structural dimensions of the back plate and the horn are adjusted to determine the final flange position and structure, as shown in Fig. 2. The pin is designed for a 3mm thick workpiece. In our investigation, the 303 austenitic stainless steel, 3Cr13 martensitic stainless steel and SKD11 tool steel are selected as the transducer materials to verify the effect of the material on the ultrasonic vibration. H13 is used as the pin material for light metal welding.

3 Elastic modulus measurement

To study the effect of metal material on the vibration characteristics and reduce the error of designed frequency, the material density, sound velocity and elastic modulus of the transducer are measured. Compared with the static measurement of the tensile machine, the non-destructive acoustic wave method is utilized to measure the elastic modulus of the material based on the principle of sound wave propagation in the solid. The shear velocity and longitudinal velocity of ultrasonic waves in the medium are as follows:

$$V_L = \sqrt{\frac{E(1-\mu)}{\rho(1+\mu)(1-2\mu)}} \tag{1}$$

$$V_T = \sqrt{\frac{E}{2\rho(1+\mu)}} \tag{2}$$

$$G = \frac{E}{2(1+\mu)} \tag{3}$$

Where ρ is the density, E is the elastic modulus, G is the shear modulus, μ is the Poisson's ratio, V_L is the longitudinal wave sound velocity, V_T is the shear wave sound velocity.

By measuring the longitudinal and shear sound velocity of the material, the elastic modulus and Poisson's ratio equation of the material are obtained [31]:

$$E = \rho V_T^2 \frac{3V_L^2 - 4V_T^2}{V_L^2 - V_T^2} \tag{4}$$

$$G = \rho V_T^2 \tag{5}$$

$$\mu = \frac{V_L^2 - 2V_T^2}{2V_L^2 - 2V_T^2} \tag{6}$$

According to the above principle, the pulse echo is to measure the elastic modulus in our experiment. By measuring the time interval Δt between the reflected echoes and the length of test piece, the equation $v=2l/\Delta t$ is calculated and the ultrasonic propagation velocity in the sample is attained. To reduce the measurement error, the cylindrical specimen is selected in 100mm length and 20mm diameter. The same heat treatment is adopted in the machining process. The material quality is measured by an electronic balance and the metal density is attained.

The ultrasonic testing device in experiment is illustrated in Fig. 3(a). The narrow pulse is generated by the signal generator (CTS-8077PR), and boosted by a power amplifier. A longitudinal wave probe (SIUI2.5Z14N) with 5MHz frequency and 10mm diameter is to receive longitudinal wave echo signals, and a shear wave probe (GE MB2Y) with 5MHz frequency and 5mm diameter is to receive shear wave echo signal, as seen in Fig. 3(c). The acoustic signals are monitored and collected by an oscilloscope. GW-III ultrasonic coupling agent and echo shear wave couplant is adopted for longitudinal and shear wave probe, separately. The longitudinal wave velocity and shear wave velocity of different material were measured 10 times and their average values were obtained.

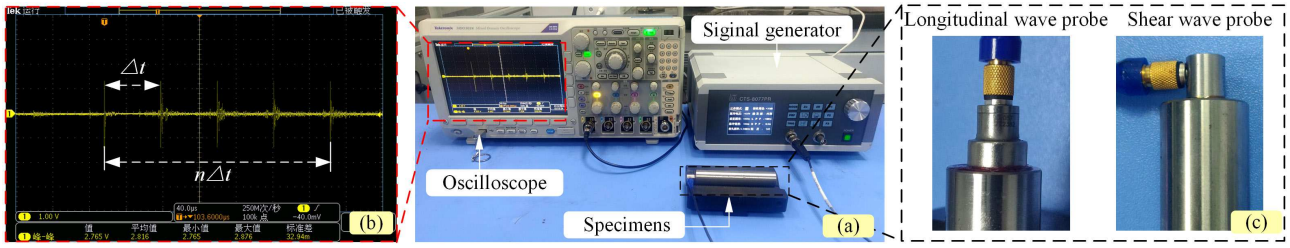

Fig. 3 Experimental platform of the elastic modulus measurement.

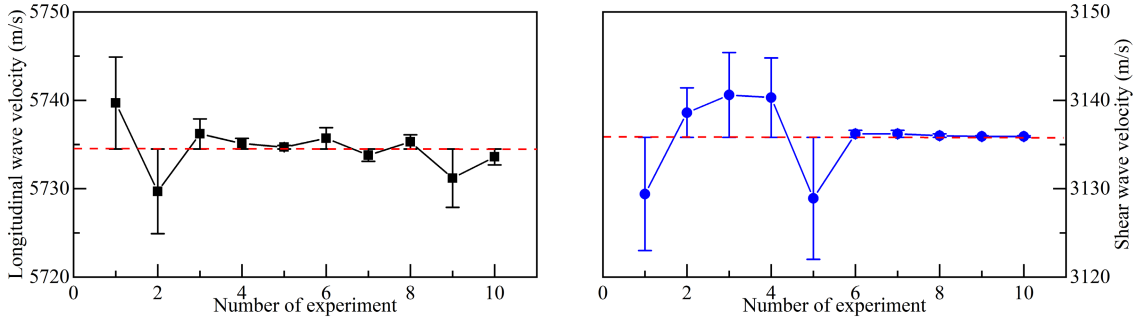

Fig. 4 Sound wave velocity: (a) longitudinal wave velocity; (b) shear wave velocity

The measurement results of longitudinal and shear velocity of 303 material are shown in Fig. 4. The wave velocity and elastic modulus of four metals are measured and listed in Table 1. It is shown that the measured elastic modulus is close to the engineering value, which proves the feasibility of non-destructive acoustic wave method. Compared with the engineering value, the maximum error for the elastic modulus is 5.6% from 3Cr13 metal, and the maximum error of density is 1.5% from H13 metal. Therefore, the engineering elastic modulus and density used in modal analysis would lead to deviation of designed frequency.

In addition, we find that the sound velocity by Eq. (1) and Eq. (7) has a significant effect on simulating calculation. If the engineering elastic modulus is calculated by the expression (1) and (7), the sound velocity is compared to the one of the non-destructive acoustic wave. It indicates that the error of sound velocity by Eq. (8) is above 12%, the sound velocity is more accurate by Eq. (1), as listed in Table 2, which is benefit to the modal design and calculation.

$$V_{L1}=\sqrt{E/\rho} \tag{7}$$

Table 1 Measured physical properties of materials

	Engineering data			Experiment data					Error	
Material	ρ (kg/m^3)	E (GPa)	μ	ρ (kg/m^3)	V_L (m/s)	V_T (m/s)	E (GPa)	μ	$\Delta\rho$ (%)	ΔE (%)
303	7930	193	0.3	7896.7	5734.5	3135.8	199.8	0.287	-0.42	+3.52
3Cr13	7760	219	0.3	7751.2	5895.6	3217.5	206.7	0.288	-0.11	-5.62
SKD11	7800	214	0.3	7689.1	5975.5	3236.4	208.2	0.292	-1.42	-2.71
H13	7800	210	0.3	7680.5	5995.4	3242.7	208.9	0.293	-1.53	-0.52

Table 2 Calculated and measured sound velocity

Material	Experiment V_L(m/s)	$V_{L1}=\sqrt{E/\rho}$ (m/s)	ΔV_{L1} (%)	$V_L=\sqrt{[E(1-\mu)]/[\rho(1+\mu)(1-2\mu)]}$ (m/s)	ΔV_L (%)
303	5734.5	4933.4	-13.97	5723.9	-0.19
3Cr13	5895.6	5312.4	-9.89	6163.7	+4.55
SKD11	5975.6	5237.9	-12.35	6077.2	+1.70
H13	5995.4	5188.7	-13.46	6020.2	+0.41

4 Finite element simulation

To obtain appropriate axial vibration mode, the resonant frequency, vibration modes, the node location, and the mounting flange structure of the transducer are investigated. Fig. 5 demonstrates the designed structure of ultrasonic transducer in our study. The length of the transducer is designed by $\lambda=V_L/f$, and the nodal point is placed in front of the piezoelectric ceramic stack. To meet with the welding of different thicknesses workpiece, the pin is designed into a two-stage section. The structure of the shoulder section can be adjusted to adapt to different workpieces.

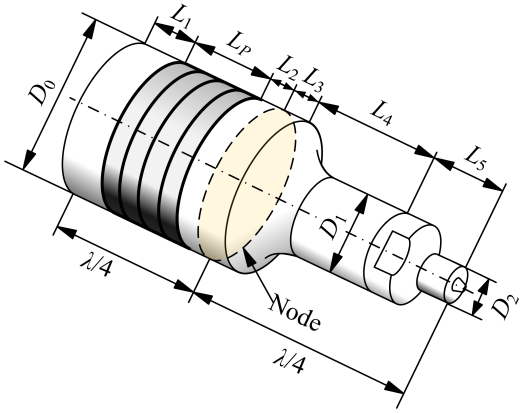

Fig. 5 Geometric diagram of flangeless transducer

The modal analysis was carried out by finite element method (FEM, ANSYS software) after the 3-D model of the transducer was established. During the simulations, the vibration frequency and mode shape are obtained by Block Lanczos solver under free boundary conditions. The material density and elastic modulus by non-destructive acoustic wave in Table 1 were introduced into the FEM model. The PZT-4 with a 7600 kg/m^3 density, 64.5 GPa elastic modulus and 0.3 Poisson's ratio is selected for the piezoceramics. It is worth noted that the three transducers are designed with the same structure to further analyze the influence of vibration output by different materials. With the modal calculation, the vibration modes of transducer with different metal are presented by adjusting the geometric dimensions of each part. As shown in Fig. 6, the resonant frequencies for three transducers are close to the 20 kHz designed frequency, which is 19698 Hz (303 metal), 19969 Hz (3Cr13), and 20049 Hz (SKD11), respectively. The transducer vibrates in the axial shape, where the maximum displacement is located at the pin tip. It is clear presented that the vibration vector of transducer is in axial direction. There is one node point along its axis vibration, which can be connected to the mounting flange structure.

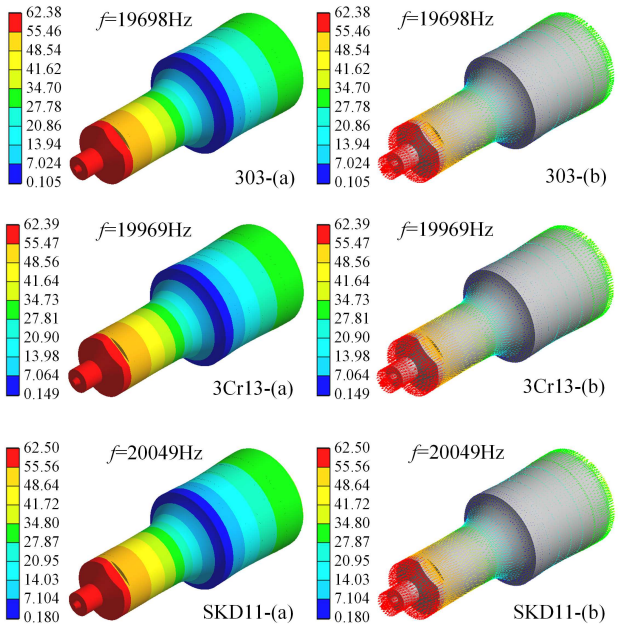

Fig. 6 Modal analysis of flangeless structure

The mounting flange structure with 3mm thickness is designed on the node surface, and the simulation result is shown in Fig. 7. Then, the mounting flange structure is connected to the BT40 holder by screws. The modal vibration of three transducers with flange structure is shown in Fig. 7(a). Its vibration modes of the transducers are in an appropriate mode, where the vibration of flange structure is close to zero. Compared to the flangeless structure, the resonant frequency of transducers with flange structure increases 200 Hz. It indicates that the structure and location of the mounting flange are designed reasonably and cannot greatly affect the frequency and vibration transmission of the transducer. The final dimensions of each part of the transducer and frequency are shown in Table 3, in which the vibration modes are normal when the three transducers are in the same size, same mounting flange and same node location. The frequencies of transducers designed by 303 steel (TRD-303), 3Cr13 steel (TRD-3Cr13) and SKD11 steel (TRD-SKD11) are 19904Hz, 20190Hz, 20273Hz, respectively. Finally, the modal analysis of the ultrasonic tool holder, is carried out by integrating with the ultrasonic transducer, the mounting flange, and the holder, and the result is

summarized in Fig. 7 (b), and (c). From the modal vibration in Fig. 7 (b) and the vibration transfer vector in Fig. 7 (c), it is observed that the vibration displacement is amplified by the horn, and the vibration is concentrated in the pin. In a whole, the vibration is close to zero for the tool holder, indicating that the vibration of the tool holder is efficiently propagated to the processing area, instead of being transmitted to the tool holder and the spindle.

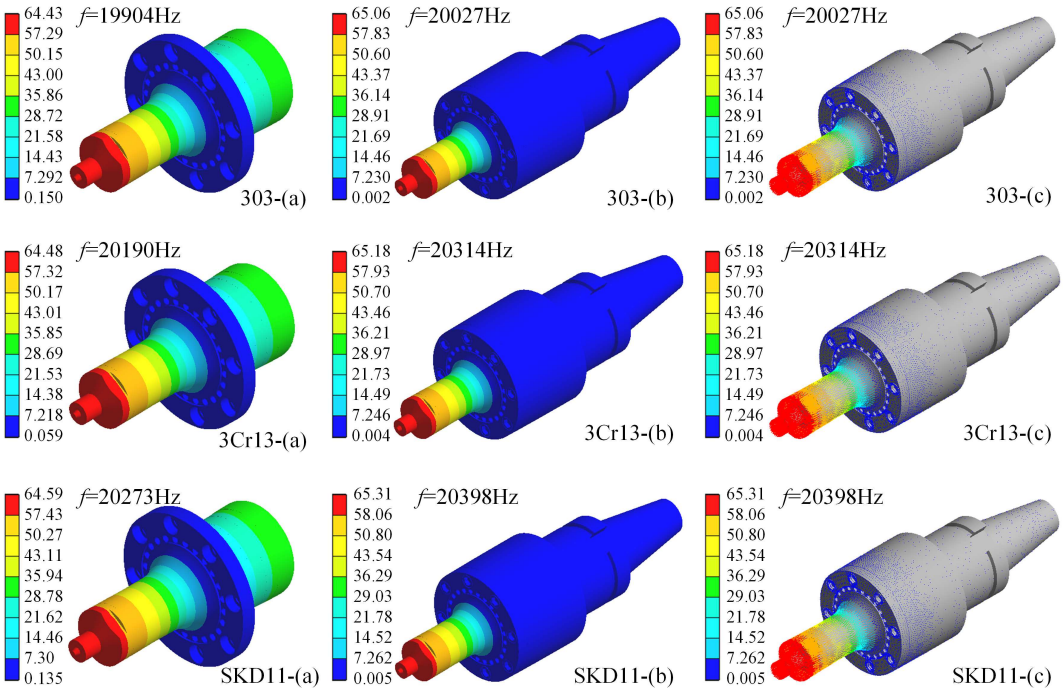

Fig. 7: (a) Longitudinal vibration mode of the transducer with flange structure, (b) Longitudinal vibration mode of the ultrasonic holder, (c) Ultrasonic transfer vector of the ultrasonic holder

Table 3 Geometries and frequency of the transducer with flange structure

Category	Parameters values (mm)									Frequency (Hz)	Vibration mode
	D_0	D_1	D_2	L_1	L_p	L_2	L_3	L_4	L_5		
TRD-303										19904	normal
TRD-3Cr13	50	30	12	13	26	6.5	3	44	23	20190	normal
TRD-SKD11										20273	normal

5 Experiments

5.1 Effect of pre-tightening on the transducer impedance

The FSW ultrasonic tool holders with three metals were fabricated and the prototypes were attained. The pre-tightening torque for the piezoceramics stack was controlled by the high-precision digital display torque wrench. Fig. 8 shows the prototype for the FSW ultrasonic tool holder after careful assembly.

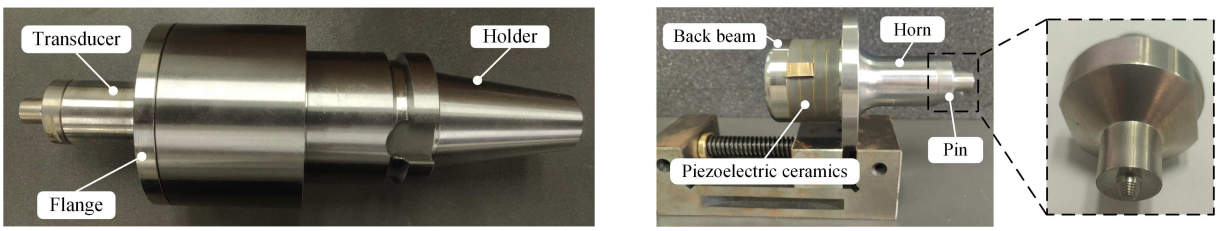

Fig. 8: (a) The FSW ultrasonic tool handle; (b) The assembled transducer

It is reported that the pre-tightening torque for transducer affects the resonant frequency, impedance, electromechanical coupling coefficient, and mechanical quality factor, thereby affecting the ultrasonic energy conversion efficiency and the vibration amplitude of the tip [30]. However, the optimum pre-tightening torque varies with the area of the piezoceramics. In this study, we use the prestress to express the pre-tightening state

between the piezoceramics and the screw. To determine the optimal prestress for piezoceramics, the relationship between resonant frequency, impedance, mechanical quality factor and pre-tightening stress were investigated. A digital torque wrench was used to apply a specific torque to the bolt, and an impedance analyzer (Agilent 4294A) was to measure the resonant frequency, impedance and electrical parameters of the transducer.

Eq. (8) and (9) established the expression of the pre-tightening stress of piezoceramics through the torque. Because the torque coefficient (K) is related to the pitch diameter, the thread lead angle, the equivalent friction coefficient of the thread, a testing platform with a precise force sensor was to test the torque coefficient, as shown in Fig. 9. The results of torque coefficients K for three transducers (303, 3Cr13, SKD11) are 0.199, 0.201 and 0.215, respectively.

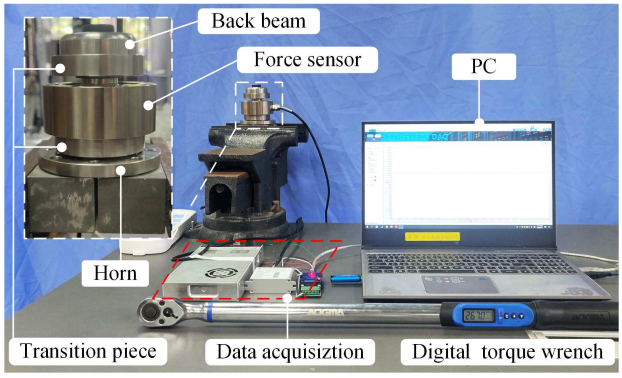

Fig. 9 Experiment of torque coefficient measurement

$$T_t = KF_0 d \tag{8}$$

$$F_0 = \sigma_{bolt} A_{bolt} = \sigma_{piezos} A_{piezos} \tag{9}$$

Where T_t is the pre-tightening torque applied to the screw bolt, F_0 is the pre-tightening force, d is the diameter of the bolt, K is the torque coefficient, A_{bolt}, A_{piezos} is bolt area and the ring area of the piezoelectric ceramic, σ_{bolt}, σ_{piezos} is the prestress of bolt and piezoelectric ceramics.

Fig. 10 presents the measured results of impedance and frequency by the pre-tightening torques from 40 N·m to 240 N·m. It is found that with the increasing of torques, the resonant frequency of the transducer increases sharply at low torque region (Fig. 10 (a), (d) and (g)), and the impedance decreases rapidly (Fig. 10(b) (e) and (f)), which is beneficial to increase the electrical current and enhance the vibration amplitude output. As an important indicator reflecting the internal friction consumption of the transducer, the mechanical quality factor (Q_m) is improved with the increasing of the torques (Fig. 10(c), (f) and (i)), which can improve the energy conversion efficiency. As the pre-tightening torque turns up to a certain level, the resonant frequency, impedance, and mechanical quality factor become into a stable level.

According to the measured torque coefficient (0.199, 0.201 and 0.215), the prestress of piezoelectric ceramic plate was obtained. The maximum prestress of the piezoceramics in this study is 50 MPa, and the piezoceramics is not depolarized and cracked under this prestress. The Fig. 10 shows that the impedance and frequency of transducer changes sharply with the increase of prestress in range of 0-20MPa. This phenomenon indicates that at the low prestress range, the piezoelectric components of the transducer are not in good connection, resulting in relative large impedance, low quality factor, even moving when vibrating. When the prestress exceeds to 30 MPa, the impedance and frequency of the transducer gradually become stable, meaning that the acoustic coupling between the transducer components is significantly improved. In Fig 10, we can control the prestress of the transducer within the range of 35-45 MPa.

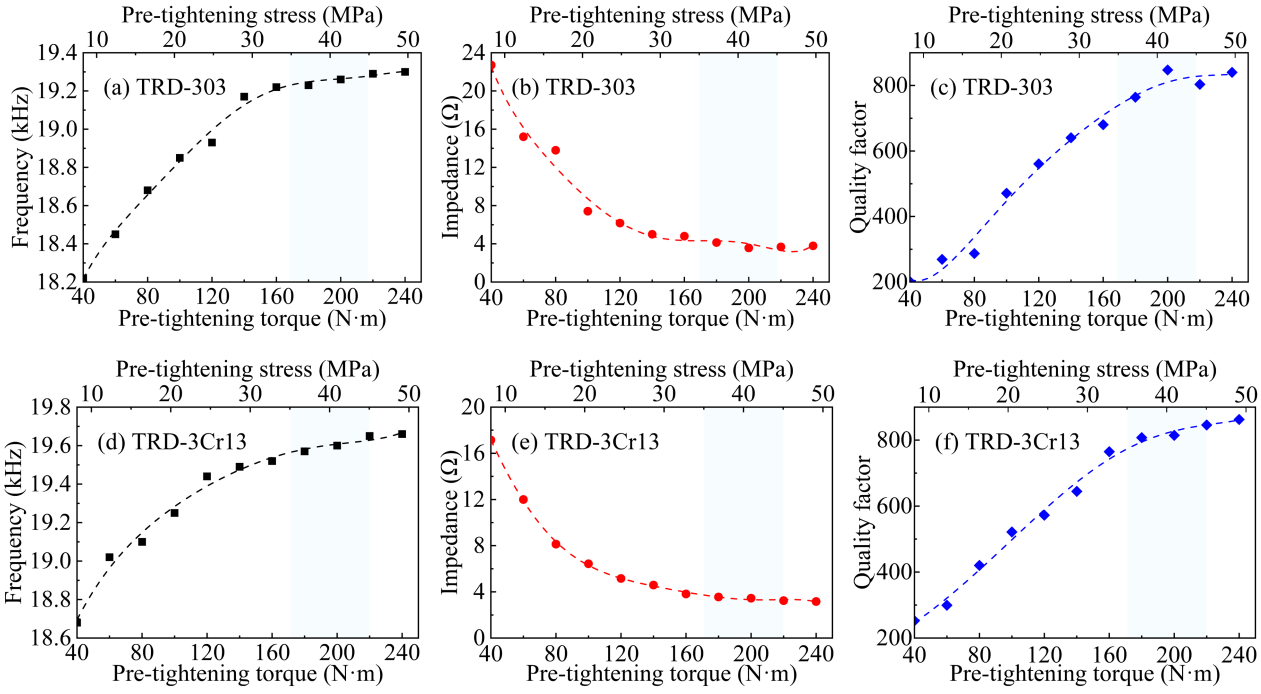

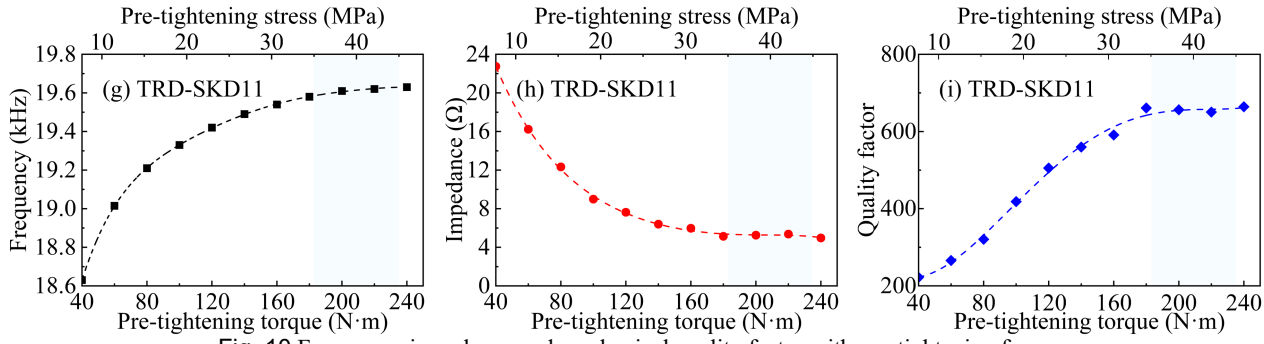

Fig. 10 Frequency, impedance and mechanical quality factor with pre-tightening force

5.2 Impedance and frequency of transducer

After the assembled transducer was aged for a long time, the impedance-phase-frequency curves of the transducers are presented in Fig. 11. The measured results demonstrate that the impedance curves of the three transducers are smooth with no parasitic resonant frequency, indicating that the longitudinal vibration can be excited well at the resonant frequency. By testing, the resonant frequency of the TRD-303 is 19900 Hz and the impedance is 4.34 Ω; the resonant frequency of TRD-3Cr13 is 20130 Hz and the impedance is 4.77Ω; the resonant frequency of the TRD-SKD11 is 20230 Hz and the impedance is 4.25 Ω. The internal resistance for three transducers is relatively low, indicating that the pre-tightening force has made good acoustic connection between the components of the transducer. The electromechanical coupling coefficient k_{eff}, which evaluates the energy conversion efficiency from electrical energy to mechanical vibration, can be calculated from Eq. (10). The electromechanical coupling coefficients of TRD-303, TRD-3Cr13, and TRD-SKD11 are attained as 33.6%, 37.5%, and 36.1%, respectively.

$$k_{eff}=\sqrt{(f_p^2-f_s^2)/f_p^2} \tag{10}$$

Where f_p is the antiresonant frequency, f_s is the resonant frequency.

In Fig. 10, with the pre-tightening torque from 40N·m to 240 N·m, the resonant frequency is increased to about 5%. As listed in Table 4, Δf_E is the error between the simulation frequency by engineering value and test frequency ($\Delta f_E=|f_E-f_s|/f_s$), Δf_A is the error between the simulation frequency by non-destructive acoustic wave and test frequency($\Delta f_A=|f_A-f_s|/f_s$). Under the appropriate pre-tightening force and the elastic modulus obtained by the non-destructive acoustic wave, the resonant frequency transducers is in a maximum error of 0.3% and within 60 Hz in frequencies. However, the maximum error of the resonant frequency calculated by the engineering value is 1.87% (377Hz). It is proved that the accuracy of designed frequency for transducer in our study can be improved when the elastic modulus and density of the material were measured accurately, and the pre-tightening stress was valuated to the connection of the ceramics materials.

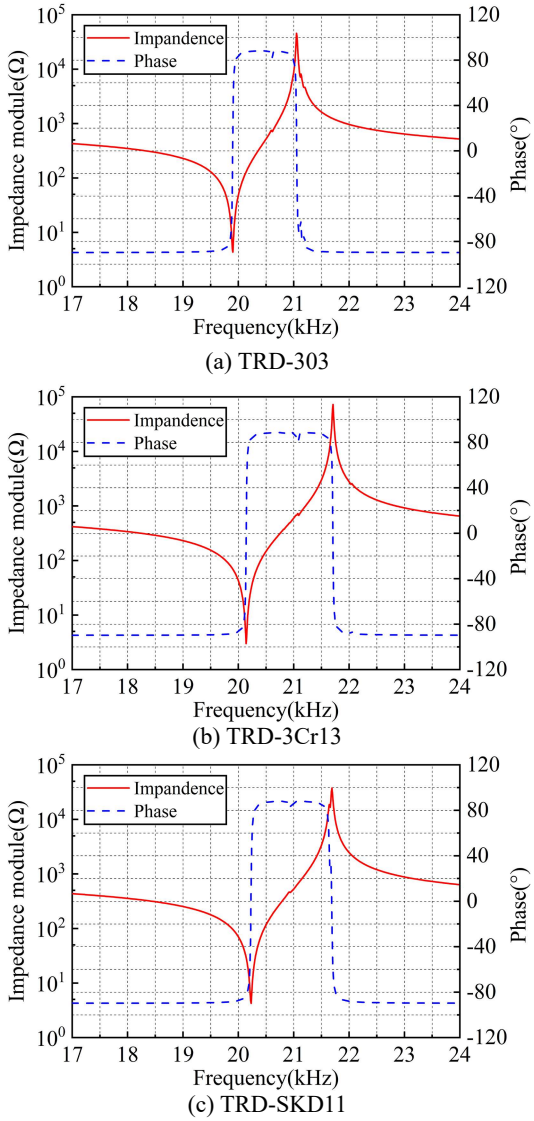

Fig. 11 The impedance-phase-frequency curves

Table 4 Comparison of the two different simulation test resonant frequency

Category	Test f_s(Hz)	Simulation frequency f_E (Hz)	Simulation frequency f_A (Hz)	Error Δf_E (%)	Error Δf_A (%)
TRD-303	19900	19687	19904	1.07	0.02
TRD-3Cr13	20130	20507	20190	1.87	0.30
TRD-SKD11	20230	20353	20273	0.61	0.21

5.3 Vibration characteristics of ultrasonic transducer

The vibration testing platform of the ultrasonic transducer are shown in Fig. 12. An excitation signal is generated from a self-developed ultrasonic generator to drive the transducers. A Laser Doppler Vibrometer (HSV-700) is to capture the vibration amplitude at the end of the transducer. The voltage and current of the piezoelectric ceramic stack are obtained at the output of the generator. Tektronix oscilloscopes are used to collect and record voltage, current and vibration signals. A hand held infrared thermometer is to monitor the temperature of the transducer.

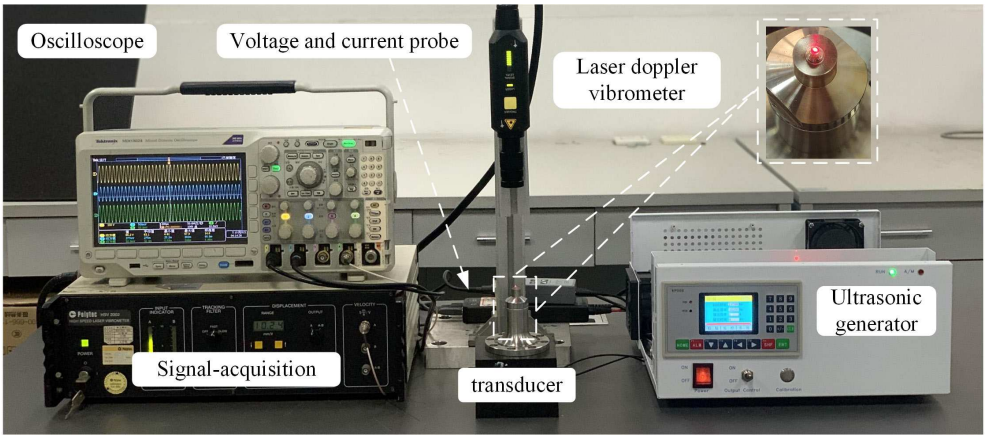

Fig. 12 The experimental system of transducer vibration

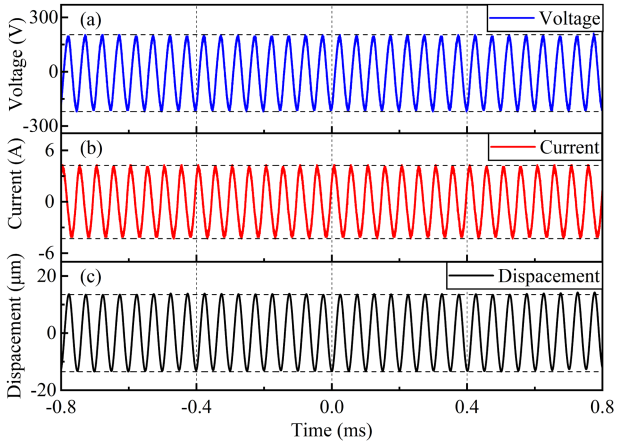

Fig. 13 The signals of the transducer: (a) the voltage, (b) the current, (c) displacement

The position of the vibration signal at the pin tip collected by the laser sensor is shown in Fig. 12. The transducer is driven by sinusoidal piezoelectric signals at different duties. The voltage, current and vibration displacement curves of the TRD-303 transducer at 50% duty is recorded. The result is in Fig. 13(a), (b) and (c), showing that the voltage, current and displacement is in a good and stable sinusoidal waveform. The PP (peak-to-peak) amplitude of the transducers along the RMS (Root Mean Square) current is presented in Fig. 14 at different duties. It is found that when the RMS current reaches to 3.5A, the PP amplitude of TRD-303, TRD-3Cr13 and TRD-SKD11 are up to 30μm, 24.0μm, and 24μm, respectively. The linear fitting curve shows a good linearity between amplitude and current.

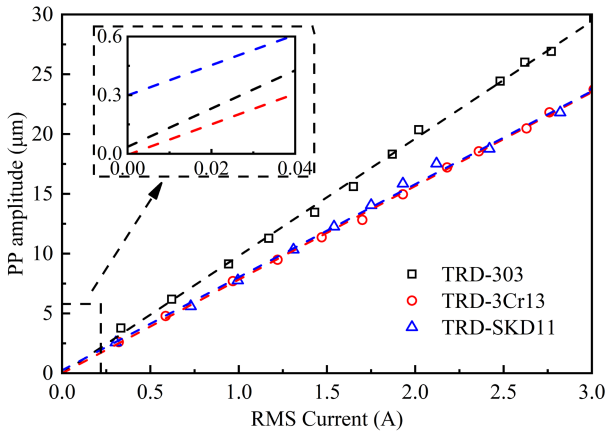

Fig. 14 The amplitude of transducers with the RMS current

5.4 Vibration characteristics of different material

As above mentioned, the three steel material transducers are designed in the same structure and same dimension, fabricated by the same prestress (40MPa). It is shown that the resonant frequency of the three transducers is within 0.33 kHz range from 19.9 kHz to 20.23kHz. Then, we evaluated the effect of the different materials on the amplitude output of the transducers. From the amplitude linear fitting curve in Fig. 13, it is found that TRD-303 can output the maximal amplitude at the same RMS current. The vibration of TRD-303 is much higher (25.9%) than the one of TRD-3Cr13 and TRD-SKD11. However, the amplitude curves of TRD-3Cr13 and TRD-SKD11 are in almost coincide, meaning that both of them have the same vibration output capacity.

As shown in Table 1, we can see that the elastic modulus and density of 3Cr13, SKD11 are close in the physical properties. Therefore, we can conclude that the

amplitude output capacity of the transducer in 3Cr13 and SKD11 is in the same level. On the contrary, the elastic modulus and density of 303 steel are different from the ones of 3Cr13 and SKD11, which might lead to higher amplitude output. Experimental results confirm that the material physical properties and material selection of the transducer have a significant effect on the amplitude output capacity of the transducer.

6 Conclusion

In this study, a novel integrated ultrasonic tool holder for FSW is proposed and designed. To reduce the design frequency error of transducer, the elastic modulus measured by non-destructive acoustic wave is applied for modal simulation. Three steel transducers were designed and manufactured. A prestress testing platform was established, and the influence of pre-tightening forces on the resonant characteristics and vibration characteristics of the transducer was investigated, and the optimal prestress range was determined. Finally, a vibration measurement was to study the vibration of the transducer. The following conclusions can be obtained,

(1) The pre-tightening force can increase the resonant frequency of the transducer, reduce the mechanical impedance, improve the acoustic electric conversion efficiency of the transducer. The optimal prestress ranges from 35 to 45 MPa. This result can also be used for piezoelectric transducers with different sizes for PZT4 in industry.

(2) Material properties have a great influence on the resonant frequency of the transducer. Based on the elastic modulus measured by the acoustic testing, the maximum frequency design error can be controlled within 0.3% by an optimal prestress. This method provides a technical guidance for the assembly of ultrasonic transducer.

(3) The PP amplitudes of the pin for three transducers can reach more than 24 μm, which meet with the FSW requirements. The transducer with 303 steel exhibits high vibration capability among the three transducers. In addition to the structural design, material selection is also a more effective way to optimize the performance of the transducer, which is one topic that we will research in future.

Statements and Declarations

Funding information:

This work is supported by the Key Research and Development Program of Guangdong Province (2020B0 90926001), National Natural Science Foundation of China (U1913215, 2175392), the National Major Scientific Research Instrument Development of China(51827811), and Basic Research Plan of Shenzhen (GJHZ20180928154402130, JCYJ20200109113429208, JCYJ20200109112803851), University Stability Support Program of Shenzhen (GXWD20201230155427003-20 200824171126002) for the financial support. Meanwhile, the authors would like to appreciate the anonymous reviewers and the editor for their valuable comments.

Competing Interests:

The authors declare that they have no known competing financial interests or personal relationships that could have appeared to influence the work reported in this paper.

Author Contributions:

Ju Jianzhong: Calculation, simulation, experiment validation, writing-original draft preparation. **Long Zhili:** Conceptualization, supervision, funding acquisition. **Ye Shuyuan:** Hardware system design, writing-review and editing. **Liu Yongzhi:** Data collection, writing-review and editing. **Zhao Heng:** Experiment testing, writing-review and editing

References

[1] Gibson BT, Lammlein DH, Prater TJ, Longhurst TJ, Cox CD, Ballun MC (2014) Friction stir welding Process, automation, and control. J Manuf Process 16(1): 56-73. https://doi.org/10.1016/j.jmapro.2013.04.002

[2] Meng XC, Huang YX, Cao J, Shen JJ, Santos JFD (2020) Recent progress on control strategies for inherent issues in friction stir welding. Prog Mater Sci 115: 1-74. https://doi.org/10.1016/j.pmatsci.2020. 100706

[3] Verma M, Ahmed S, Saha P (2021) Challenges, process requisites/inputs, mechanics and weld performance of dissimilar micro-friction stir welding (dissimilar μFSW): A comprehensive review. J Manuf Process 68: 249-276. https://doi.org/10.1016/j.jmapro.2021.05.045

[4] Texier D, Atmani F, Bocher P, Nadeau F, Chen J, Zedan Y, Vanderesse N, Demers V (2018) Fatigue performances of FSW and GMAW aluminum alloys welded joints: Competition between microstructural and structural-contact-fretting crack initiation. Int J Fatigue 116: 220-233. https://doi.org/10.1016/j.ijfatigue. 2018.06.020

[5] Zhao J, Feng J, Jian H, Wen K Jiang L Chen XB (2010) Comparative investigation of tungsten inert gas and friction stir welding characteristics of Al-Mg-Sc alloy plates. Mater Des 31(1): 306-311. https://doi.org/10.1016/j.matdes.2009.06.012

[6] Liu X, Lan SH, Ni J (2015) Electrically assisted friction stir welding for joining Al 6061 to TRIP 780 steel. J Mater Process Technol 219: 112-123. https://doi.org/10.1016/j.jmatprotec.2014.12.002

[7] Bang HS, Bang HS, Jeon GH, Oh IH, Ro CS (2012) Gas tungsten arc welding assisted hybrid friction stir welding of dissimilar materials Al6061-T6 aluminum alloy and STS304 stainless steel. Mater Des 37: 48-55. https://doi.org/10.1016/j.matdes.2011.12.018

[8] Sun YF, Konishi Y, Kamai M, Fujii H (2013) Microstructure and mechanical properties of S45C steel prepared by laser-assisted friction stir welding.

Mater Des 47: 842-849. https://doi.org/10.1016/j.matdes.2012.12.078

[9] Liu ZL, Meng XC, Ji SD, Li ZW, Wang L (2018) Improving tensile properties of Al/Mg joint by smashing intermetallic compounds via ultrasonic-assisted stationary shoulder friction stir welding. J Manuf Process 31: 552-559. https://doi.org/10.1016/j.jmapro .2017.12.022

[10] LV XQ, WU CS, Yang CL, Padhy GK (2018) Weld microstructure and mechanical properties in ultrasonic enhanced friction stir welding of Al alloy to Mg alloy. J Mater Process Technol 254: 145-157. https://doi.org/10.1016/j.jmatprotec.2017.11.031

[11] Meng XC, Jin YY, Ji SD, Yan DJ (2018) Improving friction stir weldability of Al/Mg alloys via ultrasonically diminishing pin adhesion. J Mater Sci Technol 34(10): 1817-1822. https://doi.org/10.1016/j.jmst.2018.02.022

[12] Zhao WZ, Wu CS, Su H (2020) Numerical investigation of heat generation and plastic deformation in ultrasonic assisted friction stir welding. J Manuf Process 56: 967-980. https://doi.org/ 10.1016/j.jmapro.2020.05.047

[13] Baradarani F, Mostafapour A, Shalvandi M (2019) Effect of ultrasonic assisted friction stir welding on microstructure and mechanical properties of AZ91-C magnesium alloy. Trans Nonferrous Met Soc China 29(12): 2514-2522. https://doi.org/10.1016/S1003-6326(19)65159-9

[14] Park K, Kim G Y, Ni, J (2007) Design and Analysis of Ultrasonic Assisted Friction Stir Welding. ASME 2007 International Mechanical Engineering Congress and Exposition 3: 731-737. https://doi.org/10.1115/IMECE2007-44007

[15] Kumar S, Ding W, Sun Z, Wu CS (2018) Analysis of the dynamic performance of a complex ultrasonic horn for application in friction stir welding. Int J Adv Manuf Technol 97: 1269-1284. https://doi.org/10.1007/s00170-018-2003-0

[16] Kumar S, Wu CS (2020) Suppression of intermetallic reaction layer by ultrasonic assistance during friction stir welding of Al and Mg based alloys. J Alloy Compd 827: 1-14. https://doi.org/10.1016/j.jallcom.2020.154343

[17] Lai RL, He DQ, Liu LC, Ye SY (2014) A study of the temperature field during ultrasonic-assisted friction-stir welding. Int J Adv Manuf Technol 73: 321-327. https://doi.org/10.1007/s00170-014-5813-8

[18] Amini S, Amiri MR (2014) Study of ultrasonic vibrations' effect on friction stir welding. Int J Adv Manuf Technol 73: 127-135. https://doi.org/10.1007/s00170-014-5806-7

[19] Alinaghian I, Honarpisheh M, Amini S (2017) The influence of bending mode ultrasonic-assisted friction stir welding of Al-6061-T6 alloy on residual stress, welding force and macrostructure. Int J Adv Manuf Technol 95: 1-10. https://doi.org/10.1007/s00170-017-1431-6

[20] Wu MX, Wu CS, Gao S (2017) Effect of ultrasonic vibration on fatigue performance of AA 2024-T3 friction stir weld joints. J Manuf Process 29: 85-95. https://doi.org/10.1016/j.jmapro.2017.07.023

[21] Hu YY, Liu HJ, Fujii H (2019) Improving the mechanical properties of 2219-T6 aluminum alloy joints by ultrasonic vibrations during friction stir welding. J Mater Process Technol 271: 75-84. https://doi.org/10.1016/j.jmatprotec.2019.03.013

[22] Strass B, Wagner G, Conrad C, Wolter B, Benfer S, Fuerbeth W (2014) Realization of Al/Mg-hybrid-joints by ultrasound supported friction stir welding-mechanical properties, microstructure and corrosion behavior. Adv Mat Res 966-967: 521-535. https://doi.org/10.4028/www.scientific.net/AMR.966-967.521

[23] Tarasov SY, Rubtsov VE, Fortuna SV, Eliseev AA, Chumaevsky AV, Kalashnikova TA, Kolubaev EA (2017) Ultrasonic-assisted aging in friction stir welding on Al-Cu-Li-Mg aluminum alloy. Weld World 61(4): 679-690. https://doi.org/10.1007/s40194-017-0447-8

[24] Astashev VK, Pichugin KA, Li X, Meadows A, Babitsky VI (2020) Resonant tuning of langevin transducers for ultrasonically assisted machining applications. IEEE Trans Ultrason Ferroelectr Freq Control 67(9): 1888-1896. https://doi.org/10.1109/TUFFC.2020.2991836

[25] Razavi H, Keymanesh M, Golpayegani IF (2019) Analysis of free and forced vibrations of ultrasonic vibrating tools, case study: ultrasonic assisted surface rolling process. Int J Adv Manuf Technol 103: 2725-2737. https://doi.org/10.1007/s00170-019-03718-x

[26] Gao J, Altintas Y. Development of a three-degree-of-freedom ultrasonic vibration tool holder for milling and drilling. IEEE-ASME Trans Mechatron 2019; 24(3): 1238-1247. https://doi.org/10.1109/TMECH.2019.2906904

[27] He ZY, He H, Lou J, Li YM, Li DY, Chen YZ, Liu SJ (2020) Fabrication, structure, and mechanical and ultrasonic properties of medical ti6al4v alloys part II: relationship between microstructure and mechanical properties and ultrasonic properties of ultrasonic scalpel. Materials 13(2): 1-13. https://doi.org/10.3390/ma13020284

[28] Zhang Q, Shi SJ, Chen WS (2015) An electromechanical coupling model of a longitudinal vibration type piezoelectric ultrasonic transducer. Ceram Int 41: 638-644. https://doi.org/10.1016/j.ceramint.2015.03.200

[29] Wang FJ, Zhang HJ, Liang CM, Tian YL, Zhao XY, Zhang DW (2016) Design of high-frequency ultrasonic transducers with flexure decoupling flanges for thermosonic bonding. IEEE Trans Ind Electron 63(4): 2304-2312. https://doi.org/10.1109/TIE.2015.2500197

[30] Jiang XG, Wang KQ, Zhang DY (2017) Determining the optimal pre-tightening force of a sandwich transducer by measuring resonance resistance. Appl Acoust 118: 8-14. https://doi.org/10.1016/j.apacoust.2016.11.009

[31] Markham MF (1957) Measurement of elastic constants by the ultrasonic pulse method. J Phys D-Appl Phys 8(6): 56-63. http://iopscience.iop.org/0508-3443/8/S6/312